8-15-1997

Spatiotemporal Patterns in Liquid-Liquid Taylor-Couette-Poiseuille Flow

Richard John Campero
Iowa State University

R. Dennis Vigil
Iowa State Univ, vigil@iastate.edu

Spatiotemporal Patterns in Liquid-Liquid Taylor-Couette-Poiseuille Flow

Richard John Campero and R. Dennis Vigil*

Department of Chemical Engineering, Iowa State University, Ames, Iowa 50011

(Received 30 May 1997; revised manuscript received 15 August 1997)

The vortex structure of immiscible liquid-liquid Taylor-Couette-Poiseuille flow was studied using photographic techniques. Several parameters were considered, including the feed composition and the inner cylinder rotation rate. For certain feed compositions and sufficiently large rotation rates a translating banded structure, which consisted of alternating aqueous and organic-rich vortices, persisted indefinitely. At lower rotation rates, either a spatially homogeneous emulsion evolved or sustained oscillations between the banded and homogeneous structures developed. [S0031-9007(97)04571-7]

PACS numbers: 47.54.+r, 47.20.–k, 47.32.Cc, 83.10.Lk

Hydrodynamic instabilities that occur during Taylor-Couette flow have been the subject of numerous experimental and theoretical investigations [1,2]. Most work on this problem, however, has been limited to either homogeneous single phase fluids with no applied axial flow (for exceptions, see Refs. [3–5]) or to liquid-solid systems [6,7]. Little is known about the effects on the hydrodynamic structure of adding a second immiscible liquid phase in the presence of an applied axial flow, even though such systems are employed as liquid-liquid extraction devices with high interphase mass-transfer efficiencies [8–10]. In one of the few published studies of liquid-liquid Taylor-Couette flow, the presence of the dispersed phase was found to increase the circumferential mixing [11]. In another investigation, a Taylor-Couette cell was filled with equal volumes of water and oil. At low rotation rates of the inner cylinder, Taylor vortices consisting of water separate from vortices of oil. At higher rotation rates, the oil and water become completely emulsified, and they form a single fluid in which Taylor vortices develop [12]. Under some conditions, two emulsions have been observed; every other vortex consists of an emulsion of oil with small droplets of water, while the remaining vortices contain water with many large drops of oil. In this Letter, we describe hydrodynamic structures that evolve during liquid-liquid Taylor-Couette flow in the presence of an applied axial flow (Taylor-Couette-Poiseuille flow). In particular, a kerosene-water system was studied using photographic techniques, and three operational parameters were varied: the organic phase volume fraction in the feed to the column (φ), the rotation rate of the inner cylinder (ω), and the mean column residence time (τ_{res} = volume of annulus/total volumetric flow rate of feed).

The Taylor-Couette apparatus consisted of two coaxial cylinders with a length $L = 23.5$ cm arranged horizontally along its main axis. The inner cylinder, constructed of stainless steel, had a radius of 1.11 cm (R_1), and the outer cylinder, constructed of Lucite, had a radius of 1.27 cm (R_2), thereby giving a radius ratio $\eta = R_1/R_2$ and an aspect ratio $\Gamma = L/(R_2 - R_1)$ of 0.875 and 148, respectively. The entire assembly was surrounded by a transparent Lucite box containing water held at a constant temperature of 5 °C by a circulating water bath. The inner cylinder was driven by a Compumotor brushless motor system which enabled the acceleration ($a = 1$ rev/s^2) and the rotation rate of the inner cylinder ($\omega = 26$ to 60 rps) to be precisely controlled. If the two phase system were to behave as a homogeneous fluid with the physical properties of either water or kerosene, the circumferential Reynolds numbers corresponding to these rotation rates would range from $17.4 < \text{Re}/\text{Re}_c < 40.2$ (water) or $6.0 < \text{Re}/\text{Re}_c < 13.9$ (kerosene), where Re_c is the critical Reynolds number for the onset of laminar Taylor vortex flow. For inner cylinder rotation rates lower than $\omega = 26$ rps, the density difference between the kerosene and water led to a poorly developed vortex structure with significant radial and azimuthal density gradients. Therefore, only rotation rates with $\omega \geq 26$ were considered.

The organic phase (kerosene dyed with Oil Red O) and an aqueous phase (deionized water) were separately supplied to one end of the initially water-filled column through a manifold by two precision piston pumps. By adjusting the flow rate of each phase, the volume fraction of the organic phase, φ, and the column residence time, τ_{res}, could be accurately controlled. The effluent exited through an identical manifold at the opposite end of the cell. For each experiment, the inner cylinder was first accelerated to the desired speed, and the inlet pumps were started. A color video camera and VCR were used to record the spatial distribution of kerosene in the column. After data collection was complete, a time-lapse movie was created by assembling images from the video tape, acquired at

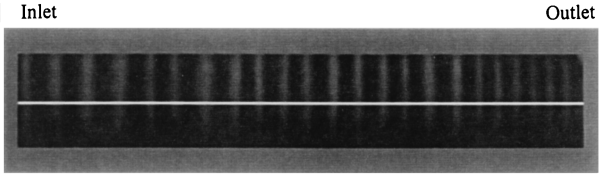

FIG. 1. A single captured movie frame. Pixels under the white line were extracted from each frame and assembled into an image to produce Figs. 2–4.

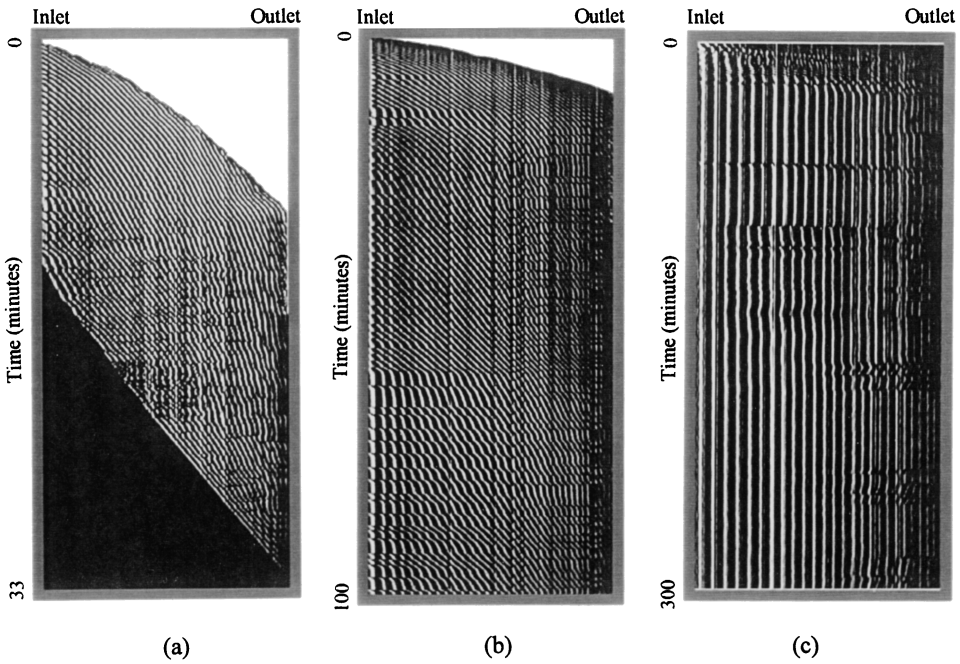

FIG. 2. Evolution of the vortex structure for $\varphi = 0.40$ and $\tau_{\text{res}} = 20$ min. The feed streams enter from the left side of the image. Time increases along the vertical axis from top to bottom. (a) $\omega = 32$ rps; (b) $\omega = 48$ rps; (c) $\omega = 60$ rps.

intervals of 1 or 2 sec. Figure 1 is an example of such a movie frame; the inlet of the cell is located at the left side, and the outlet is located at the right end. To concisely show how the spatial structure changes with time, axial slices of each movie frame (with a width of 1 pixel) were assembled row by row into an image file and converted to gray scale (Figs. 2–4).

In all experiments, the initial flow pattern that evolved after start-up consisted of two types of alternating Taylor vortices: kerosene-dispersed vortices and water vortices. The kerosene-rich vortices appear black in the axial length versus time images (Figs. 2–4), whereas the water vortices are white. After the formation of this banded structure was complete, three distinct categories of behavior were observed under different operating conditions: (1) The alternating vortex structure moved in the same direction as the imposed axial flow, but not at the same velocity of the bulk fluid flow, (2) a phase inversion occurred so that kerosene became the continuous phase and there was no longer any spatial variation in the Taylor vortices, or (3) the vortex structure in the column alternated periodically between the banded and the homogeneous inverted states described above. To unmask spatial structure in the inverted state that may be obscured by the dye in the kerosene, separate experiments were performed using an aqueous phase dyed with spectracid red and a dye-free kerosene phase. These experiments confirm the observation that the inverted state consists of spatially homogeneous vortices of water droplets dispersed in kerosene.

A phase diagram for these various structures in $\varphi - \omega$ parameter space is shown in Fig. 5 for a fixed axial flow rate ($\tau_{\text{res}} = 20$). Column phase inversion was favored for large kerosene volume fractions and at moderate rotation rates; the alternating (banded) vortex structure was observed at low kerosene volume fractions and for high cylinder rotation rates. For example, Figs. 2(a), 2(b), and

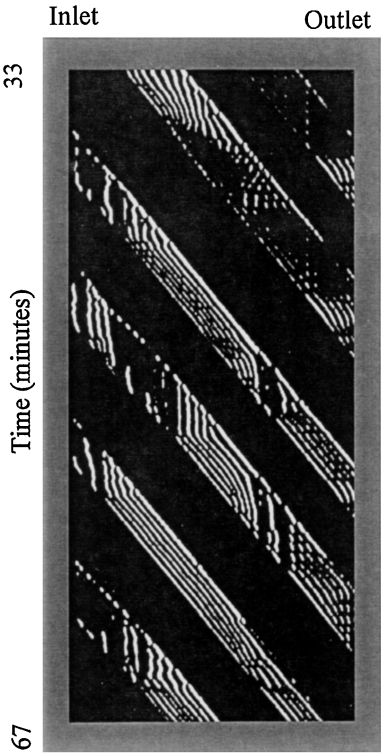

FIG. 3. Evolution of the vortex structure for $\varphi = 0.32$, $\omega = 32$ rps, $\tau_{\text{res}} = 20$ min.

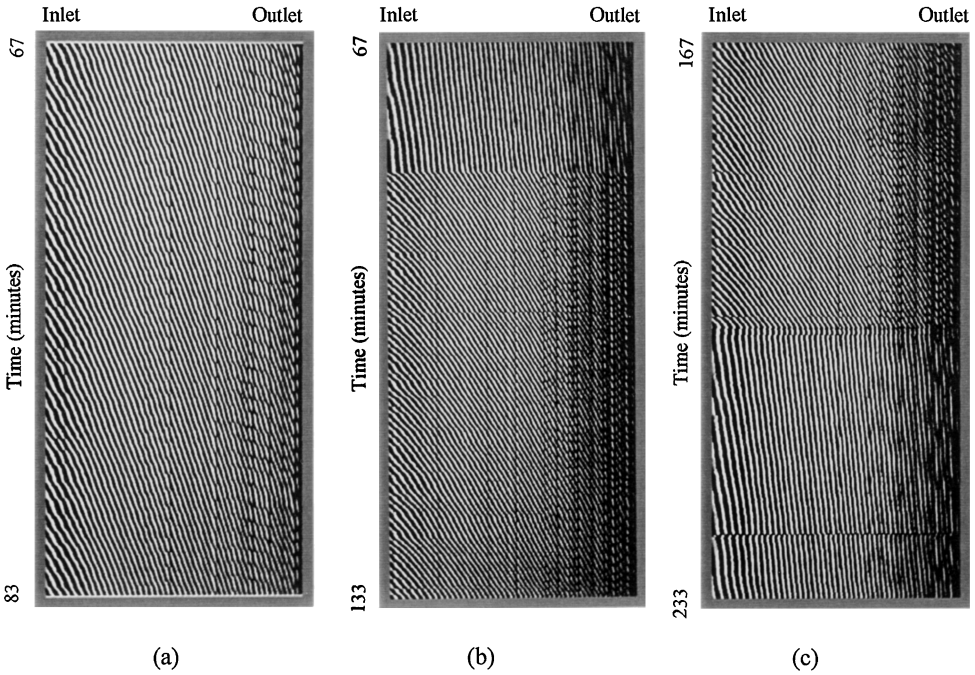

FIG. 4. Evolution of the axial vortex structure for $\varphi = 0.10$ and $\omega = 32$ rps; (a) $\tau_{\text{res}} = 20$ min; (b) and (c), $\tau_{\text{res}} = 40$ min.

2(c) show the evolution of the vortex structure for $\tau_{\text{res}} = 20$ min and $\omega = 32$, 48, and 60 rps, respectively. Figure 2(a) is an example of column phase inversion. Initially, the banded structure moved through the column from the inlet to the outlet. However, after approximately 13.5 min, a phase inversion occurred at the column inlet. The inversion propagated through the column at a steady velocity (nearly identical to the space velocity), overtaking each vortex and leaving in its wake homogeneous vortices consisting of an emulsion of water droplets dispersed in kerosene. Figures 2(b) and 2(c) are examples of the banded structure, which is observed at higher rotation rates. For $\omega = 48$ rps, no phase inversion was observed, and the system retains an axially translating alternating vortex structure. When the rotation rate of the inner cylinder was further increased from 48 to 60 rps, the kerosene bands did not move axially except for small perturbations near the outlet. The wavelength and width of the kerosene-rich vortices also increased noticeably as the rotation rate of the inner cylinder was increased. The axial velocity of the kerosene-rich bands (V_b) relative to the mean space velocity ($V_d = V_b/V_s$, where V_s = volume flow rate at inlet/cross-sectional area) also depended upon axial position, and some of these velocities are listed in Table I for selected experimental conditions. Figure 3 illustrates an example of oscillations between the inverted state and the banded vortex structure, which occurs at relatively low rotation rates and large kerosene volume fractions. Notice that the width of the banded and homogeneous inverted regions remain relatively constant throughout the duration of their passage through the column.

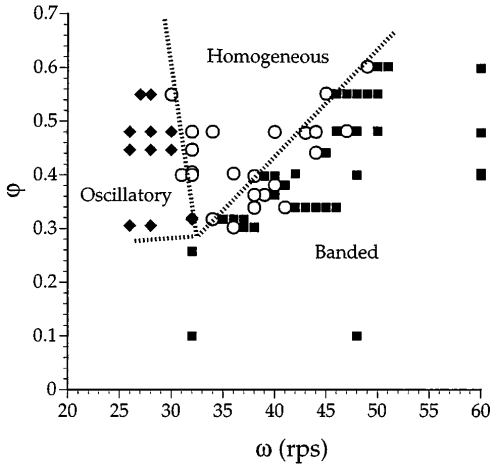

FIG. 5. Phase diagram in $\varphi - \omega$ parameter space and for $\tau_{\text{res}} = 20$ min. The phase boundary between the inverted and banded states is shown for decreasing rotation rates only.

The transitions between the various states described above were studied by performing experiments with the usual water-filled initial condition and subsequently increasing and/or decreasing ω. No hysteresis was detected on the boundary between the homogeneous inverted state and the oscillatory state. In contrast, the phase boundary between the homogeneous inverted state and the banded

TABLE I. Kerosene band velocity normalized by V_s.

φ	τ_{res}	ω	V_d Inlet	V_d Middle	V_d Outlet
0.1	20	32	1.32	0.80	0.75
0.4	20	60	Vortex bands stationary		
0.4	40	32	0.10	0.24	0.28
			Velocity of inversion/V_s = 0.98		

structure did depend upon whether ω was being increased or decreased. In particular, if the system was initially in the inverted state and ω was increased, the banded structure was not observed for any value of ω. If the system was initially in the banded state and ω was decreased, the transition to the homogeneous inverted state was the same as that shown in Fig. 5.

In the experiments discussed above, only the feed composition and rotation rate were varied, whereas the imposed axial flow rate was fixed. However, several experiments were also performed in order to determine the effect of changing τ_{res} on the vortex structure, and some of these results are shown in Fig. 4. For $\tau_{\text{res}} = 20$ min and $\omega = 32$ rps, the velocity and width of the kerosene bands decrease over the length of the column and the vortex structure becomes time independent after start-up transients decay [Fig. 4(a)]. However, when τ_{res} was increased to 40 min [Figs. 4(b) and 4(c)], the velocity of the bands changed discontinuously between two values. At times, the axial velocity of the bands was greater than the mean space velocity; at other times the velocity of the bands was much smaller than the space velocity. At least three such sudden changes in velocity were observed over the duration of the experiment (6 h). Further experiments are needed to determine if the switching between the two velocities occurs at periodic intervals.

A limited number of experiments have also been performed to elucidate the effects of changing the relative density of the two fluids on the vortex structure. In particular, the kerosene ($\rho = 0.79$ g/cm^3) was replaced with silicone oil ($\rho = 0.97$ g/cm^3), which has a density nearly identical to that of water. As in the case of the kerosene-water system, at high rotation rates the alternating banded vortex structure was observed; for lower rotation rates and sufficiently large silicone oil volume fractions, the system evolved to the homogeneous inverted state. Apparently, the translating banded vortex structure does not arise from the density difference of the working fluids alone, but instead depends upon other physical properties.

The findings discussed above suggest the existence of at least two instabilities: (1) A transition from an axially translating spatially inhomogeneous banded structure to a homogeneous emulsion occurs as either ω is decreased or φ is increased, and (2) a transition from the spatially homogeneous vortex structure to the oscillatory state occurs as ω is decreased. In addition, we have observed that the velocity of the axially translating banded structure decreases with increasing rotation rate; for sufficiently large rotation rates the axial velocity vanishes. Perhaps the most surprising of these findings is that a homogeneous emulsion was produced at lower cylinder rotation rates (for fixed τ_{res} and φ), whereas a well ordered spatial structure evolved at higher cylinder rotation rates. Also, in the two-phase system considered in this work, the vortices do not generally move at the space velocity, and in some cases they do not move at all. Since an axial flow is imposed on the system, the axial transport must occur by some mechanism other than by simple convection and diffusion. Perhaps the strongly turbulent nature of the vortices studied here gives rise to anomalous diffusive processes. However, for sufficiently small axial flow rates, axial transport in single phase Taylor-Couette-Poiseuille flow can be well represented by diffusion-convection equations with the Taylor vortices translating at the mean space velocity [3,13]. Future tracer-response studies will provide insight into the mechanism of axial transport in these cases.

Several important questions about the nature of the hydrodynamic structures described in this Letter merit further study. For example, little is known about the effects of the physical properties of the two fluids on the bifurcation structure. Some of these are currently being explored, including the density ratio, viscosity ratio, and interfacial surface tension.

*Author to whom correspondence should be addressed.

[1] R. C. Di Prima and H. L. Swinney, in *Hydrodynamic Instabilities and the Transition to Turbulence*, edited by H. L. Swinney and J. P. Gollub (Springer-Verlag, Berlin, 1985), 2nd ed.
[2] *Ordered and Turbulent Patterns in Taylor-Couette Flow*, edited by C. David Andereck and F. Hayot, NATO ASI Series, Ser. B, Vol. 297 (Plenum, New York, 1992).
[3] K. Kataoka, H. Doi, T. Hongo, and M. Futagawa, J. Chem. Eng. Jpn. **8**, 472 (1975).
[4] A. Tsameret and V. Steinberg, Phys. Rev. Lett. **67**, 3392 (1991).
[5] K. L. Babcock, D. S. Cannell, and G. Ahlers, Physica (Amsterdam) **61D**, 40 (1992).
[6] T. Imamura, K. Saito, and S. Ishikura, Polym. Int. **30**, 203 (1993).
[7] K. Kataoka, N. Ohmura, M. Kouzu, Y. Simamura, and M. Okubo, Chem. Eng. Sci. **50**, 1409 (1995).
[8] M. W. Davis, Jr. and E. J. Weber, Ind. Eng. Chem. **52**, 929 (1960).
[9] G. J. Bernstein, D. E. Grosvenor, J. F. Lenc, and N. M. Levitz, Nucl. Tech. **20**, 200 (1973).
[10] R. A. Leonard, G. J. Bernstein, R. H. Pelto, and A. A. Ziegler, AIChE J. **27**, 495 (1981).
[11] J. Legrand and F. Coeuret, Chem. Eng. Sci. **41**, 47 (1986).
[12] D. D. Joseph, K. Nguyen, and G. S. Beavers, J. Fluid Mech. **141**, 319 (1984).
[13] C. M. V Moore and C. L. Cooney, AIChE J. **41**, 723 (1995).